DOE/ER/25053-2

Courant Institute of
Mathematical Sciences

U.S. Department of Energy

The Laminar to Slug Flow Transition in Hele-Shaw Flow

J. Glimm, W. Guo, and Q. Zhang

Research and Development

Supported by the Applied Mathematical Sciences
subprogram of the Office of Energy Research,
U.S. Department of Energy under
Grant DE-FG02-88ER25053

athematics and Computers

ptember 1989

NEW YORK UNIVERSITY

NYU DOE/ER 25053-2
Glimm, James
The laminar to slug flow
transition in Hele-Shaw
flow. c.2

DOE/ER/25053-2

Courant Institute of Mathematical Sciences
New York University

The Laminar to Slug Flow Transition in Hele-Shaw Flow

J. Glimm,* W. Guo,** and Q. Zhang**

Supported by the Applied Mathematical Sciences
subprogram of the Office of Energy Research,
U. S. Department of Energy under
Grant DE-FG02-88ER25053

---

* J. Glimm is at the State University of New York, Stony Brook.

** W. Guo and Q. Zhang are at the Courant Institute, New York University.

Table of Contents

Page

Abstract 1

1. Introduction 2

2. Initiation of Instability 4

3. Instability Growth 6

4. Pinch Off and Bubble Generation in a Uniform Channel 13

5. Variable Channel Width and Complex Barriers 22

6. Conclusions 25

7. Appendix. The transverse velocity field of the nonuniform flow 25

References 28

DISCLAIMER

This report was prepared as an account of work sponsored by an agency of the United States Government. Neither the United States Government nor any agency thereof, nor any of their employees, makes any warranty, express or implied, or assumes any legal liability or responsibility for the accuracy, completeness, or usefulness of any information, apparatus, product, or process disclosed, or represents that its use would not infringe privately owned rights. Reference herein to any specific commercial product, process, or service by trade name, trademark, manufacturer, or otherwise, does not necessarily constitute or imply its endorsement, recommendation, or favoring by the United States Government or any agency thereof. The views and opinions of authors expressed herein do not necessarily state or reflect those of the United States Government or any agency thereof.

Printed in U.S.A.

Available from

National Technical Information Service
U.S. Department of Commerce
5285 Port Royal Road
Springfield, VA 22161

THE LAMINAR TO SLUG FLOW TRANSITION IN HELE-SHAW FLOW

James Glimm [1, 2]
Department of Applied Mathematics and Statistics
SUNY at Stony Brook
Stony Brook, NY 11794-3600

Wei Guo [1, 2]
Qiang Zhang [2]
Courant Institute of Mathematical Sciences
New York University
251 Mercer Street
New York, NY 10012

ABSTRACT

Foam generation is a promising method to increase the efficiency of enhanced oil recovery processes. The present study began with the observation that the pinch off of bubbles upstream of an obstacle (pore throat) is a mechanism for bubble (i.e. foam) generation. We find support for this mechanism through a study of the laminar to slug flow transition in an idealized physical and geometrical setting. Transitions between multiphase flow regimes are of basic interest. A surprising conclusion of our study is the reversal of fingering stability caused by a strong transverse flow field.

Key words. Fingering, Slug Flow.

AMS(MOS) subject classifications. 76-04, 76T05, 76S05

---

[1] Supported in part by the National Science Foundation, grant DMS - 8619856

[2] Supported in part by the Applied Mathematical Sciences subprogram of the Office of Energy Research, U. S. Department of Energy, under contract DE-FG02-88ER25053

1. Introduction

This study is motivated by the problem of foam generation, which is a promising method to increase the efficiency of enhanced oil recovery (EOR) processes. The foam serves to retard flow in high mobility, or conduction channels, and it thereby increases the efficiency of the EOR process in contacting low permeability portions of the petroleum reservoir. Our study began with the observation [6] that the pinch off of bubbles upstream of an obstacle (a pore throat in the rock matrix) was a mechanism for bubble formation. We find support for this mechanism, which we examine in simplified physical and geometrical settings. As we now discuss, the transitions between distinct multiphase flow regimes are also of interest to fundamental science and provide a further motivation for the present study.

We regard multiphase flow regimes as phases, in the sense that within each regime, the constitutive law which defines the multiphase flow equations varies smoothly, while along the boundary between the distinct regimes, which may occur abruptly in the state space of the flow parameters, such as the void fraction, the equilibrium constitutive relations may change discontinuously.

From this point of view, a multiphase flow problem we have studied extensively, namely Rayleigh-Taylor instability [3, 5], can be regarded as a metastable transition between bubbly and slug flow. The study of the bubble envelope, or the outer layer between the mixing layer and the ambient heavy fluid, is dominated by bubble merger, which is the microscopic mechanism for the bubbly flow to slug flow transition. The effort to discuss metastable phenomena using only equilibrium state variables leads typically to complex characteristics and imaginary sound speeds, while a direct analysis of nonequilibrium thermodynamics leads to new dependent variables, whose dynamics is a rate law. For the Rayleigh-Taylor problem, the new dependent variable is the bubble size at the bubble envelope. The formulation of a rate law lies at the heart of the proposed statistical models [9, 10, 14] and is also closely related to the much studied formula $h = \alpha A g t^2$ for the acceleration of the bubble envelope [7].

In the present work, we make no connection to the averaged multiphase flow equations and we investigate instead the dynamics at the level of individual bubbles and slugs. Studies of this nature have as their objective the definition of constitutive laws and rate laws, i.e. the definition of equilibrium and nonequilibrium thermodynamics of multiphase flow. Within this microscopic framework, we study in detail a mechanism leading to a transition to slug flow. Our approach is to seek a consistent picture, combining simple theoretical arguments with first principle computations based on the front tracking method [4]. Other approaches to multiphase flow are presented in [1, 2, 12, 13].

The simplified physics we consider is that of miscible displacement in two dimensions, i.e. Hele-Shaw flow. The equations for two fluid Hele-Shaw flow are

$$v = -\mu_i^{-1} \nabla P \ , \quad i = o, s \ , \tag{1.1}$$

$$\nabla \cdot v = 0 \ .$$

Here the two fluids are denoted oil (o) and solvent (s), while μ_i is the viscosity of the oil or solvent. The boundary between the two fluids is assumed sharp and it moves with the velocity v. v is discontinuous across the interface, but its normal component is continuous, so that the interface motion is well defined. P denotes pressure.

It is well known that these equations are unstable on all length scales [8] and can develop essential singularities in finite time [11]. In this sense, microscopic physics (surface tension or capillary pressure) will regularize the flow. Often, and this is the point of view assumed here, the regularizing length scales are small relative to computational length scales, and so regularization can be safely achieved on numerical grounds. This small length scale limit is appropriate to flow on a reservoir or inter-well spacing length scale, but is not the correct description of flows on the scale of laboratory rock samples or of rock pores. In this sense, our equations are a simplification of the relevant physical equations.

The geometry as well as the physics is simplified in this study. We consider in order of increasing complexity, flow in a uniform channel, in a channel of variable cross section, around a simplified obstacle, and around a random array of obstacles.

A surprising conclusion of this paper is the reversal of fingering stability caused by the strong transverse flow field. In other words, we find fingers formed when the heavy (more viscous) fluid, i.e. oil, displaces the light fluid.

2. Initiation of Instability

After simplification, the problem of flow in a uniform channel has three dimensionless parameters. These are the mobility ratio $M = \frac{\mu_o}{\mu_s}$, the ratio $V = \frac{v_o}{v_s}$ of the in flow velocities v_i and the fractional oil channel width $W = \frac{w_o}{w_o + w_s}$. See Figure 2.1a. We assume $M > 1$. This is no loss of generality, as the opposite case is handled by an interchange of the two fluids. There is no flow through the upper or lower channel boundaries, the in and out flow rates at left or right boundaries are assumed to be constant in each fluid, and the total in flow and out flow must be equal by incompressibility. The total flow is a constant, which can be removed from the problem by rescale of the time variable. Thus the boundary conditions are set by the ratios of the in flow and out flow fluid velocities. This simple geometry is modified by a small barrier near the inlet, separating the two flow channels. The equation $MV = 1$ defines an equilibrium (laminar) solution. The in flow velocities or the dimensionless ratio V is taken to be arbitrary, while the out flow velocity ratio $V_{\text{out}} = \frac{v_o}{v_s}$, and hence the out flow velocities themselves, are assumed to be determined from the equation $MV_{\text{out}} = 1$.

The regime $MV > 1$ corresponds to excess oil flowing into the channel, as is shown in Figure 2.1, while the regime $MV < 1$ corresponds to excess solvent. In either case, for $MV \neq 1$, the initial conditions do not correspond to a solution of the flow equations, and the resulting transients are the object of this study.

To understand the details of the pinch off phenomena, we first consider the $t = 0$ velocity field, $v(t = 0)$. This field can be represented as a sum of two terms, $v = v' + (v - v')$, the first of which is a uniform flow field v', coinciding with the out flow (right) boundary conditions. This field is purely horizontal, and is M times as large in the solvent as in the oil. The second term, $v - v'$, is a nonuniform flow field, which has zero out flow boundary conditions, and has net in flow of oil and net out flow of solvent at the left boundary, if $MV > 1$. Otherwise, if $MV < 1$, the in flow and out flow at the left boundary are reversed. From this picture, see Figure 2.1(b), the nonuniform flow field $v - v'$ causes entrainment of the fluid with excess in flow into the other flow channel. In other words, the $t = 0$ velocity will give rise to the initiation of a finger into the channel which is deficient in flow. In contrast to the Taylor-Saffman theory, the finger is transverse to the channel flow produced by v'.

To measure the strength of the pinch off we introduce the ratio γ of the nonuniform flow to uniform flow,

$$\gamma_i = \frac{v_i - v_i'}{v_i'} \qquad i = o,\, s \quad . \tag{2.1}$$

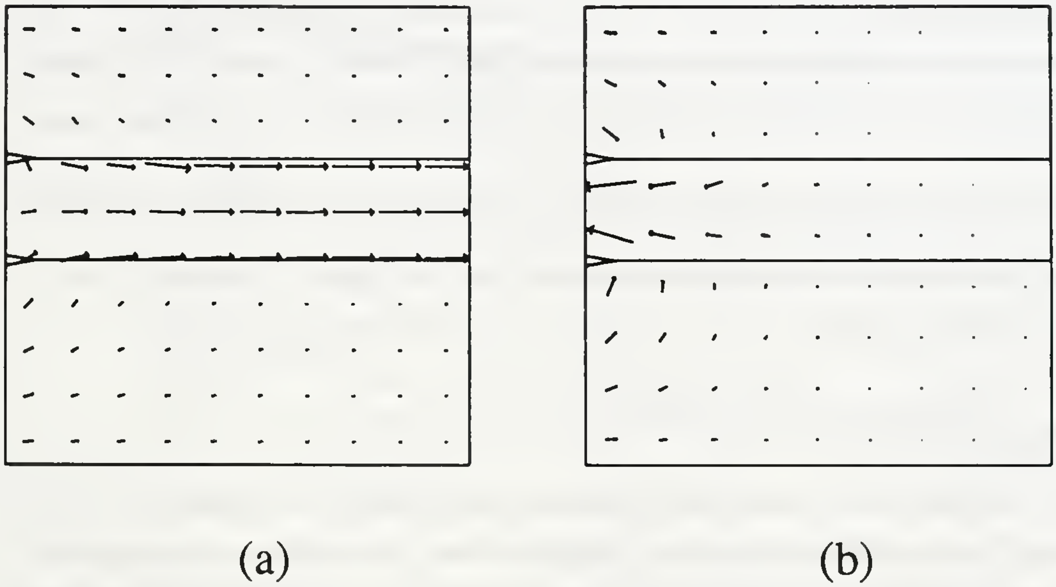

Figure 2.1. The central channel is solvent located between two layers of oil. (a) The velocity field of the total flow v. The injection rate on the right boundary satisfies $MV = 1$. The left boundary velocity ratio V is larger than the equilibrium value, i.e. $MV > 1$, which results in excess in flow of oil. (b) The velocity field of the nonuniform flow $v - v'$. There is no flow across the right boundary. The excess oil in flow produces the transverse field which drives the solvent flow backward at the inlet. As the transverse field of the nonuniform flow is strong, a small part of the solvent flow in the computational domain may be driven back into the inlet. For this reason, two small inlet barriers which separate the oil and solvent in flows were installed to avoid this situation.

Then γ_o can be expressed by terms of M, V and W as follows

$$\gamma_o = \frac{(1 - W)(MV - 1)}{1 + W(V - 1)} \quad . \tag{2.2}$$

To study the nonuniform flow $v - v'$, we examine the variation of $\delta v_y = v_y - v'_y$ along the interface. For two cases, $W = .5$ and in the asymptotic limit of large M, it is possible to determine the behavior of v_y analytically, as we show in Appendix A, namely

$$v_y = K \ln \left[\frac{1 + \exp(-\pi x / 2WH)}{1 - \exp(-\pi x / 2WH)} \right] , \tag{2.3}$$

where $K = -\dfrac{\mu_1 \delta v_1 - \mu_2 \delta v_2}{\pi(\mu_1 + \mu_2)}$ with $\delta v_i = v_i - v_i'$ for $W = 0.5$ and $K = \gamma_o v'_o$ for large M.

In the cases when (2.3) is valid, we conclude that for small x, v_y is approximately proportional to $\ln x$, except that the singularity at $x = 0$ has been removed by the insertion of the inlet barrier between the two inlet regions. For large x, v_y decays like $e^{-\frac{\pi x}{2WH}}$, so that the nonuniform vertical flow due to excess oil flow is mainly limited to the region $0 \le x \le \dfrac{2WH}{\pi}$. Beyond this region, the flow is approximately equal to its uniform value v' given by the right boundary conditions. Therefore the length scale $\dfrac{2WH}{\pi}$ measures the of horizontal penetration distance of the nonuniform flow. In Figure 2.2, we plot v_y vs. x along the interface, and display the effects of change in M, W and V on v_y.

3. Instability Growth

Fingers growing into a strong transverse flow have qualitative features not present in the classical Taylor-Saffman instability. In this section, we construct a simple model of a square wave finger in a strong transverse flow field and give an approximate analysis to predict the main features of this flow. We then present a study of the exact solution of the Hele-Shaw flow, for fingering into a transverse flow field, and use the simple model analysis to understand the observed behavior of the computed solutions of the full Hele-Shaw equations.

The initiation of fingering was discussed in the previous section, and is caused by the nonequilibrium ($MV_{\text{in}} \neq 1$) inflow boundary conditions. We distinguish two cases. For excess inflow of the more viscous fluid (oil), we find a series of narrow fingers, repeating in a quasi-periodic or chaotic pattern for an extended time period. Depending on their length and the width of the other channel, the fingers may or may not grow to an amplitude which causes pinch off, i.e. slug flow, as is discussed in §4. For excess inflow of the less viscous fluid (solvent), we find a smooth transition to a laminar flow in which the solvent channel widens as one moves downstream, and approaches its equilibrium width, i.e. a width for which the resulting fluid velocities satisfy $MV = 1$.

The patterns in these two cases are somewhat surprising, since narrow fingers are produced in the Taylor-Saffman stable case, while wide fingers or nonfingering behavior occurs in the Taylor-Saffman unstable case.

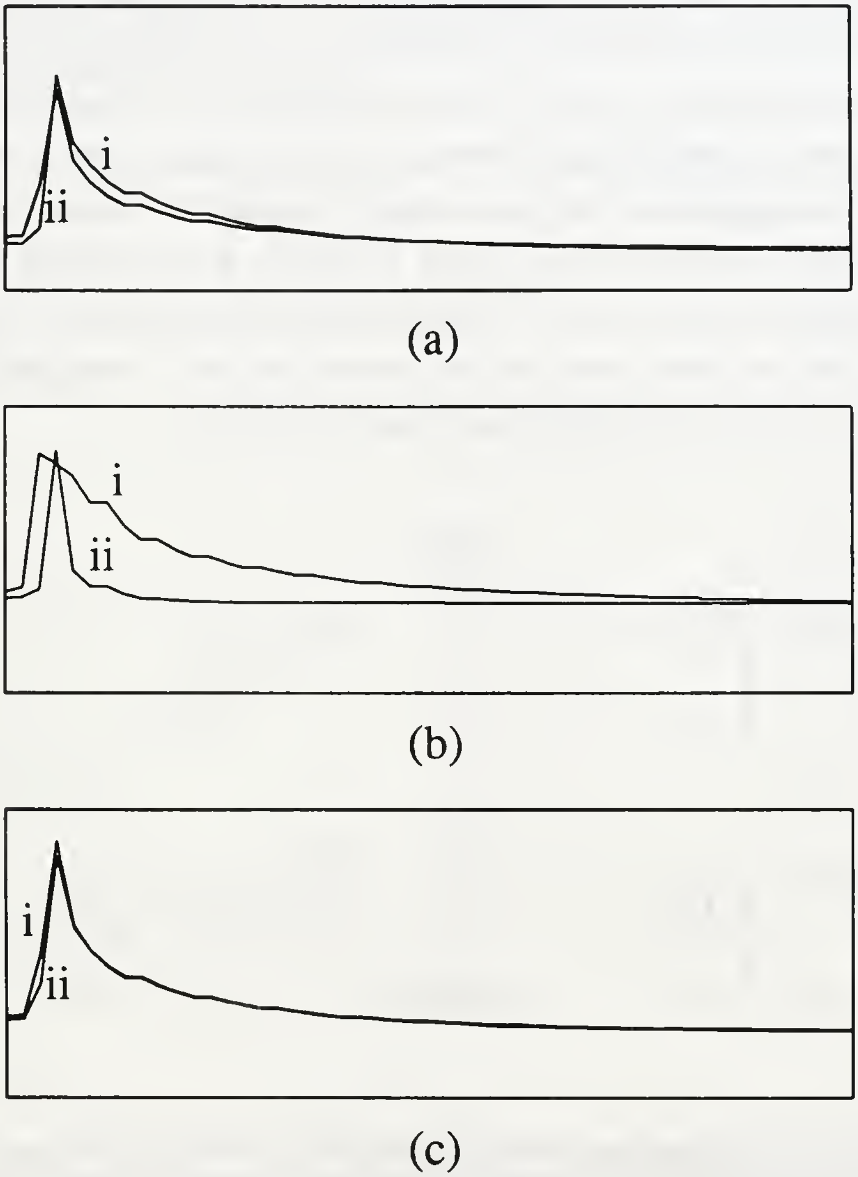

Figure 2.2. The velocity component v_y vs. x plotted along the $t = 0$ interface for the internal $0 \le x/H \le 1.5$. Each plot displays the effect of variation of one of the three parameters M, W and V. The two curves are rescaled in each case to have the same maximum height. (a) i) M = 40, ii) M = 1. For both cases V = 1.25, W = 0.5. (b) i) W = 0.9, ii) W = 0.1. For both cases V = 1.25, M = 40. (c) i) V = 0.25, ii) V = 1.25. For both cases M = 40, W = 0.5.

The simple model replaces the finger by a square wave. The dynamics of the square wave is then replaced by a one dimensional noninteracting layer ansatz, in which three horizontal layers are each treated as independent. The layers with no finger have a purely linear pressure. In the layer with excess inflow, the pressure will have a slope with a larger magnitude. In the layer with the finger, there are two cases to consider. For a more viscous finger (oil) in a less viscous ambient, the finger is a region of very steep pressure gradient. For a less viscous finger in a more viscous ambient, the finger is a region of very small pressure gradient. In terms of the horizontal motion in the layer and Darcy's law, the oil finger is entrained in a rapid flow, and is moving rapidly, so has a large velocity and large pressure gradient. The solvent finger is entrained in a region of relatively slow flow, so has small pressure drop across it. The results of these pressure fields are shown schematically in Figure 3.1. We see that for the more viscous finger, there is reenforcement of the basic finger growth on the upstream side and a cancellation on the downstream side. For the solvent finger these trends are reversed.

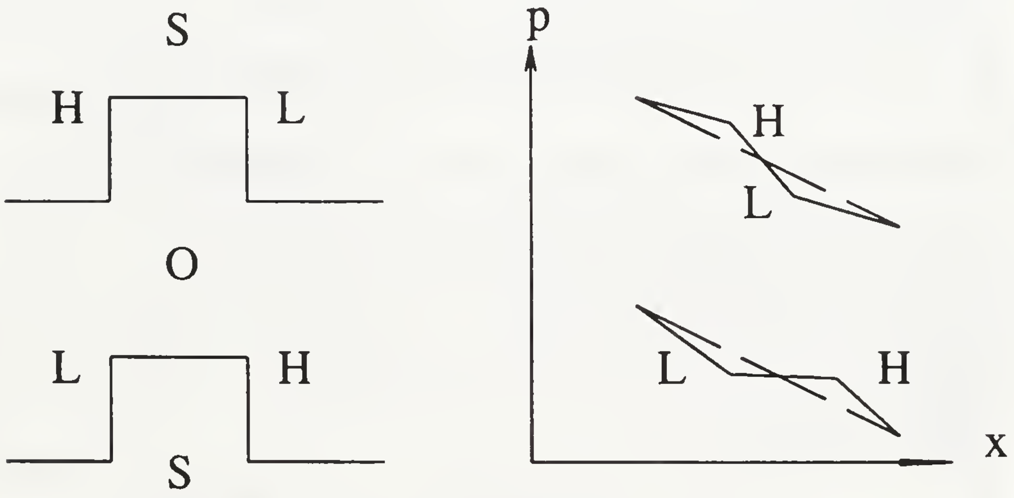

Figure 3.1. The one dimensional noninteracting layer ansatz. Schematic finger shapes and pressure fields are displayed. The dash lines represent the unperturbed pressure fields and the solid lines represent perturbed pressure fields. *H* and *L* denote the high and low pressure sides of the finger respectively.

The result of this picture is that the oil finger is transported downstream, and grows longer on its upstream side only. The solvent finger has only very slow transport, and grows on its down stream side primarily. Furthermore, the Taylor-Saffman instability of the solvent finger contributes to its down stream growth while the Taylor-Saffman stability of the oil finger yields a very reduced tendency for down stream growth. For this reason, we get narrow, long fingers of oil, and broad fingers of solvent. The solvent fingers rapidly approach an equilibrium configuration, in which the relative width of the two channels adjusts until the condition $MV = 1$ is achieved. The oil fingers move down stream, allowing the instability to re-establish itself near the inlet, and new fingers to form, in a quasi-periodic or chaotic manner.

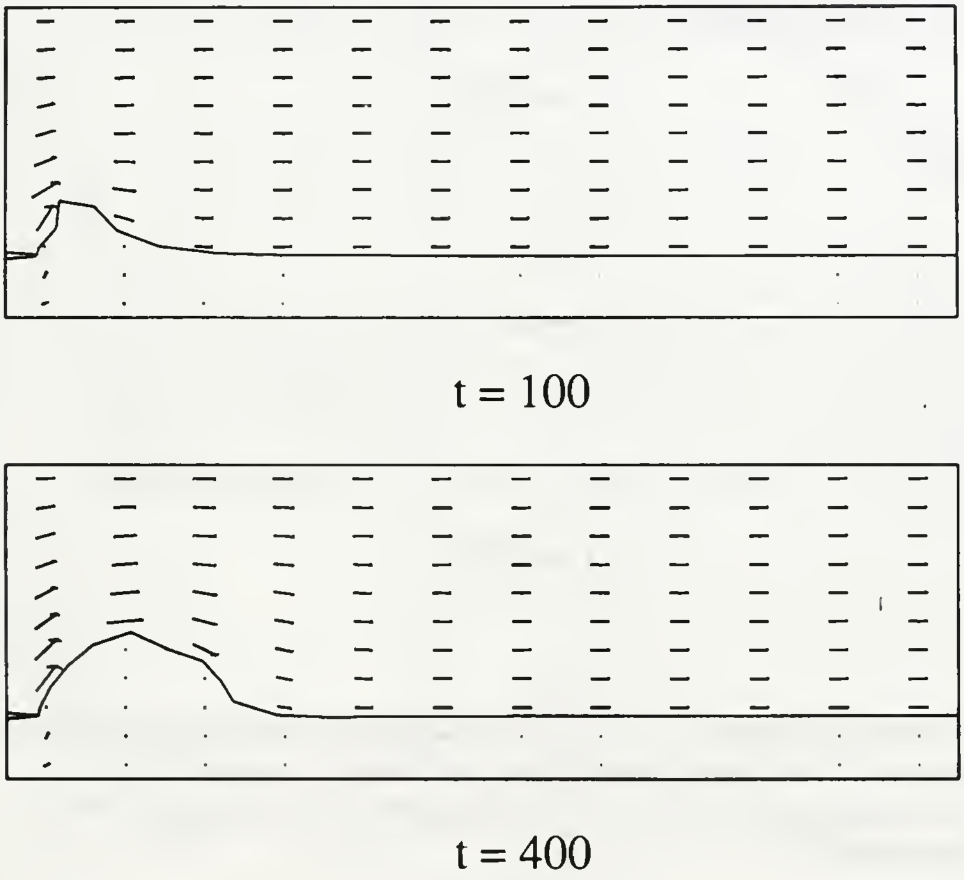

Figure 3.2. Excess in flow of oil in the bottom channel causes the growth of the oil finger into the solvent channel. We have shown two time steps for the growing finger at $t = 100$ and $t = 400$. The mesh size is 70×30 for the elliptic (pressure) equation.

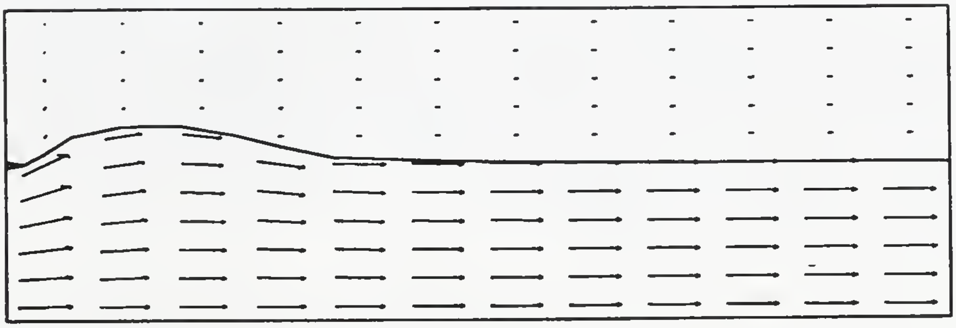

t = 400

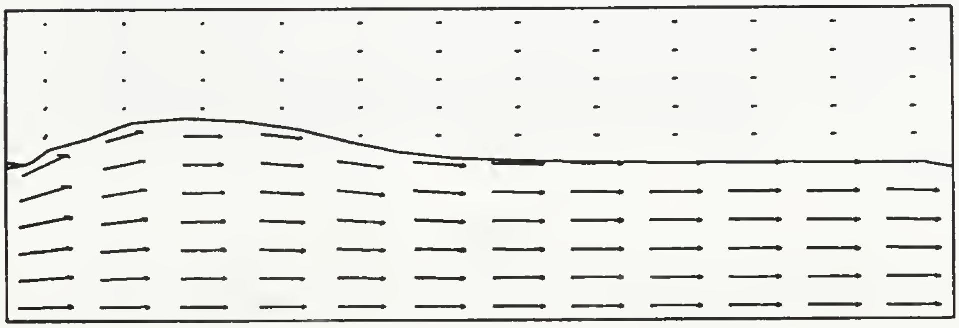

t = 600

Figure 3.3. Excess in flow of solvent in the bottom channel causes the growth of the solvent finger into the oil channel. We have shown two time steps $t = 400$ and $t = 600$ for the growing finger. The mesh size is 41×17 for the hyperbolic equation and 70×30 for the elliptic equation.

Next we examine the solution of the full Hele-Shaw equations in these two cases. In Figure 3.2 we show time frames presenting the interface positions for excess oil inflow, while Figure 3.3 treats excess solvent inflow. We see a pattern of interface development as predicted above. To continue this analysis, we show in Figure 3.4 the pressure fields, plotted as a function of x, along fixed values of y, at constant t. These figures should be compared to the qualitative discussion given at the beginning of this section. Then we compare the y component of the velocity, also plotted vs. x, along $y = \text{const.}$ lines at the same fixed t in Figure 3.5.

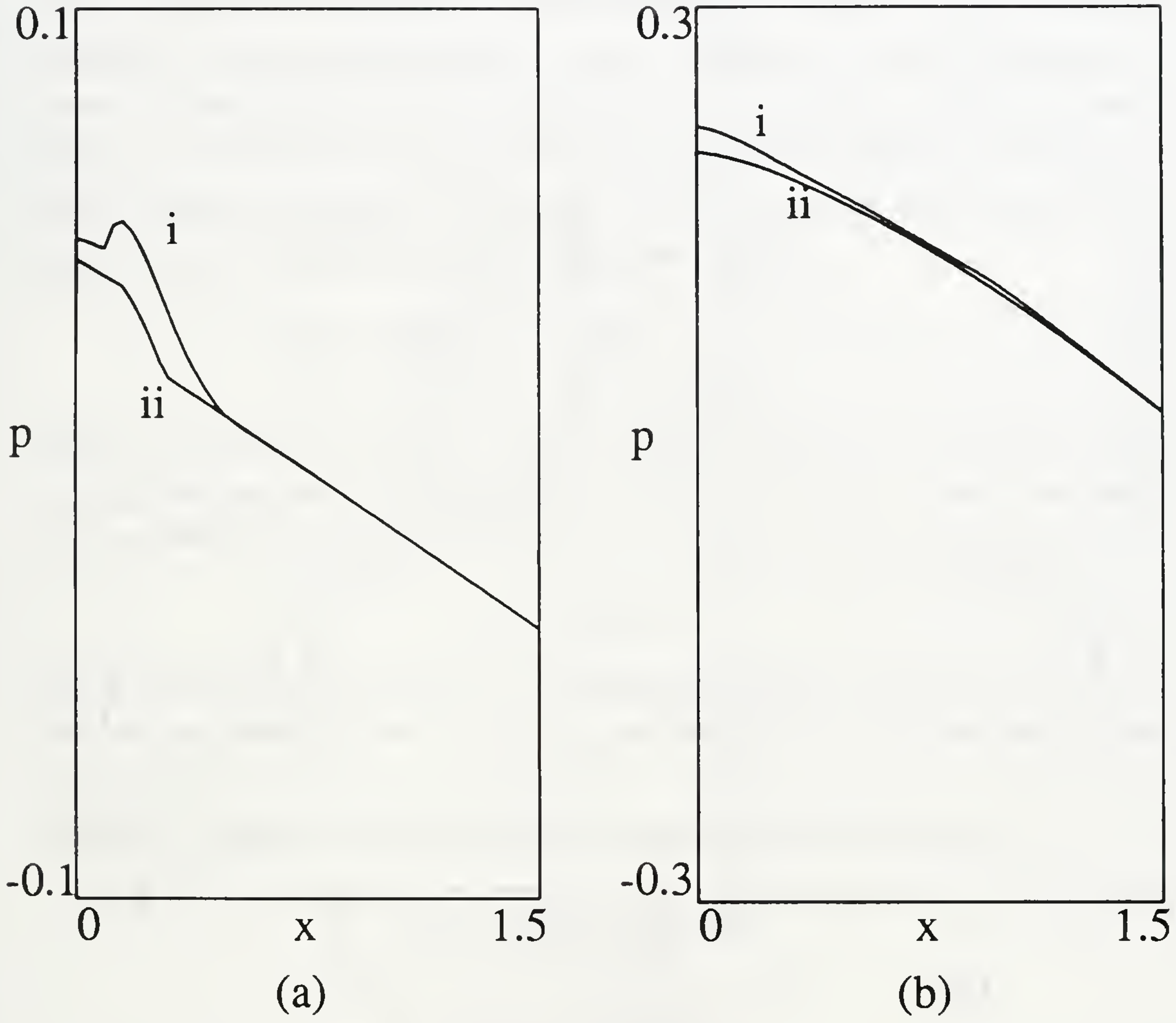

Figure 3.4. We plot pressure fields vs. x along two horizontal lines at dimensionless heights (i) $y/H = 0.2$ and (ii) $y/H = 0.3$ above the $t = 0$ interface position. (a) Excess oil inflow. $t = 100$. Inside the finger, the slope of the pressure curve is steeper than outside. (b) Excess solvent inflow. $t = 600$. Inside the finger, the slope of the pressure is smaller than on the outside. Also the slope of the pressure is smaller in front of the finger, indicating a stagnant region in front of the finger. The small slope of curve (i) near $x = 0$ and the non monotone portion of (i) in Figure 3.4a is due to the influence of the small barrier separating the flow channels near $x = 0$.

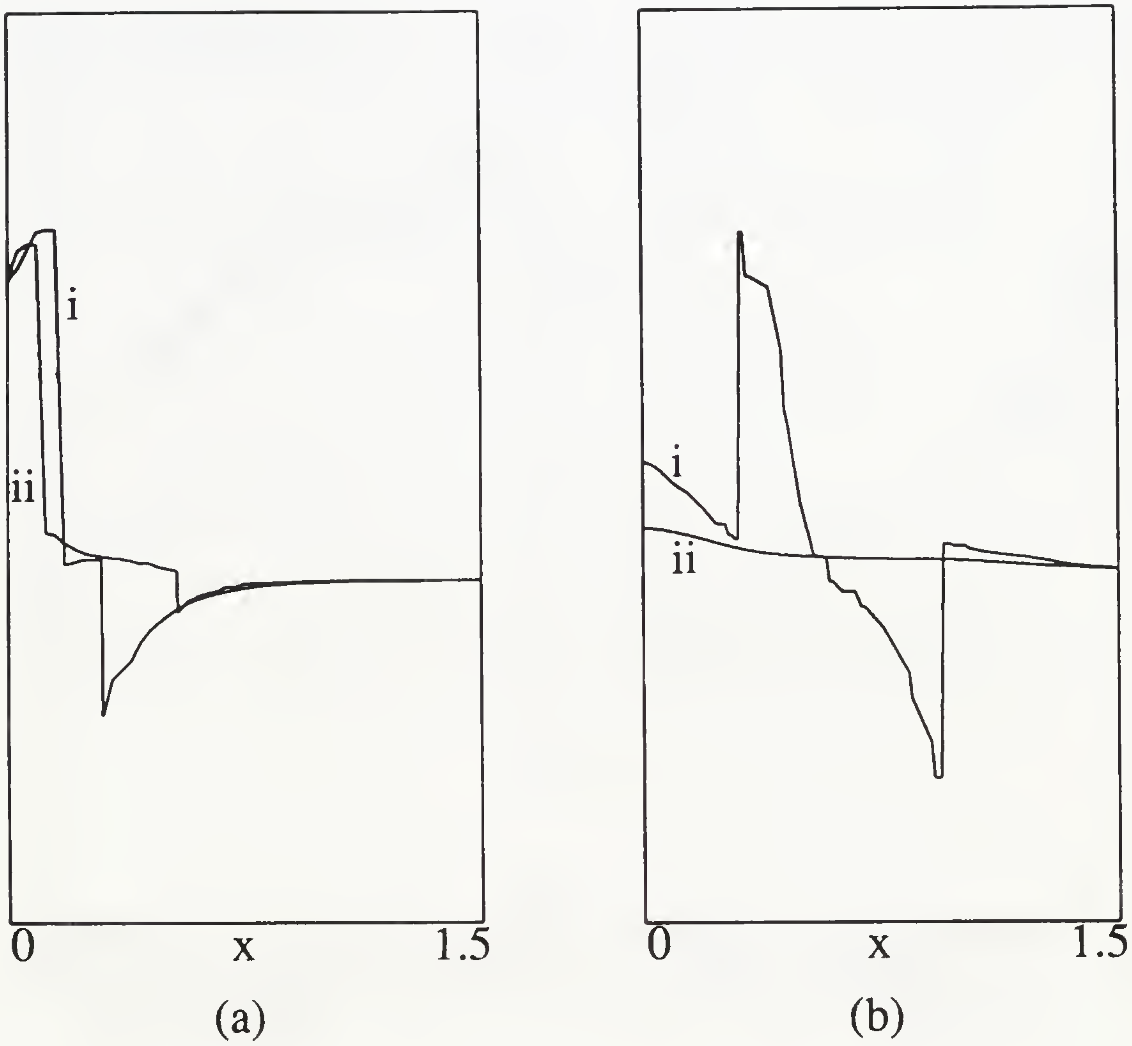

Figure 3.5. Plots of v_y vs. x along horizontal lines and times coinciding with the plots of Figure 3.4. The discontinuity in the plot occurs at the interface between the oil and the solvent.

The results we have shown from Figures 3.2 to 3.5 are not sensitive to mesh refinement. We obtained almost identical results after doubling the number of the grid lines.

4. Pinch Off and Bubble Generation in a Uniform Channel

In general terms, we find that for $MV > 1$, (2.2) gives $\gamma_o > 0$. The system deviates from equilibrium, and the excess oil in flow produces a transverse velocity field which drives the oil into the solvent channel, as shown in Figure 2.2. To describe the physical process of pinch off, there are two natural time scales to consider. The first is the pinch-off time t_p, which is the characteristic time for a single finger to grow to the height of the channel width and the second is the time t_s, which characterizes the expansion of the finger. To study t_p, we approximate the shape of the finger by

$$y(x,\ t) = \frac{4A(t)}{3\pi}\left[\frac{x_0(t)}{(x - x_0(t))^2 + x_0^2(t)}\right] \ , \quad x > 0 \quad , \tag{4.1}$$

where $A(t)$ is the area of the finger. By conservation of mass and incompressibility, $A(t)$ is equal to the total flux of the nonuniform flow $v - v' = \gamma v'$ into the channel with excess flow,

$$A(t) = WH\gamma_o {v_o}' t \quad . \tag{4.2}$$

Here H is the height of the entire flow channel and x_0 defines a half width for the finger. Since the area covered by $y(x,\ t)$ in (4.1) in the interval $0 < x < x_0$ is one third of total, we define $x_0(0)$ as follows: the nonuniform flux $v - v'$ crossing this interval at $t = 0$ is the same ratio. Therefore in case of large M according to the theory of §2, we have

$$\frac{\int_0^{x_0} \ln\frac{1+\exp(-\pi x/2WH)}{1-\exp(-\pi x/2WH)}dx}{\int_0^{\infty} \ln\frac{1+\exp(-\pi x/2WH)}{1-\exp(-\pi x/2WH)}dx} = \frac{1}{3} \quad .$$

By this definition of x_0, we find that

$$x_0(0) = 0.175WH \quad .$$

Since the oil finger penetrates into the rapid moving solvent channel, its width expands with time. As an approximation, we assume that the expansion rate is constant with time and proportional to the uniform solvent velocity. Therefore

$$x_0(t) = 0.175WH + \zeta {v'}_s t \ , \qquad 0 < \zeta < 1, \tag{4.3}$$

where ζ is a dimensionless parameter. We found that adjusting $\zeta = \zeta(W)$ to depend on W only, $\zeta \simeq 0.2$, it is possible to obtain a good fit for simulations covering a wide range of values of V, M and W. The height of the finger is given by

$$h(t) = \frac{4A(t)}{3\pi x_0(t)} = \frac{4WH\gamma_o v'_o t}{3\pi(\,0.175WH + \zeta v'_s t\,)} \tag{4.4}$$

In Figures 4.1, 4.2a and 4.2b we compare the interface and height of the oil finger calculated by (4.1) and (4.4) with the results of numerical simulations. The equation (4.4) defines a threshold, or maximum, for the finger height, h_T, which is

$$h_T = \frac{4\gamma_o v'_o WH}{3\pi\zeta v'_s} = \frac{4\gamma_o WH}{3\pi\zeta M} \quad . \tag{4.5}$$

Pinch off occurs only when the solvent channel width is less than the finger threshold, see Figure 4.1b. Therefore we have a condition for occurrence of pinch off,

$$(1 - W) < \frac{4\gamma_o W}{3\pi\zeta M} \quad . \tag{4.6}$$

The pinch off time t_p is defined by setting the finger height (4.4) to the height of the solvent channel $h_s = (1 - W)H$, yielding

$$t_p = \frac{0.175WHM\,(1 - W)}{\left[\dfrac{4W\gamma_o}{3\pi} - \zeta(1 - W)M\right] v'_s} \quad . \tag{4.7}$$

When the pinch-off occurs repeatedly, it turns a laminar flow of solvent into slug flow. To estimate approximately the slug size, we introduce the dimensionless length scale

$$\alpha = \frac{t_p v_s}{H} \quad . \tag{4.8}$$

Over a range of simulations, we find this length scale to characterize the size of the initial slug within 50%.

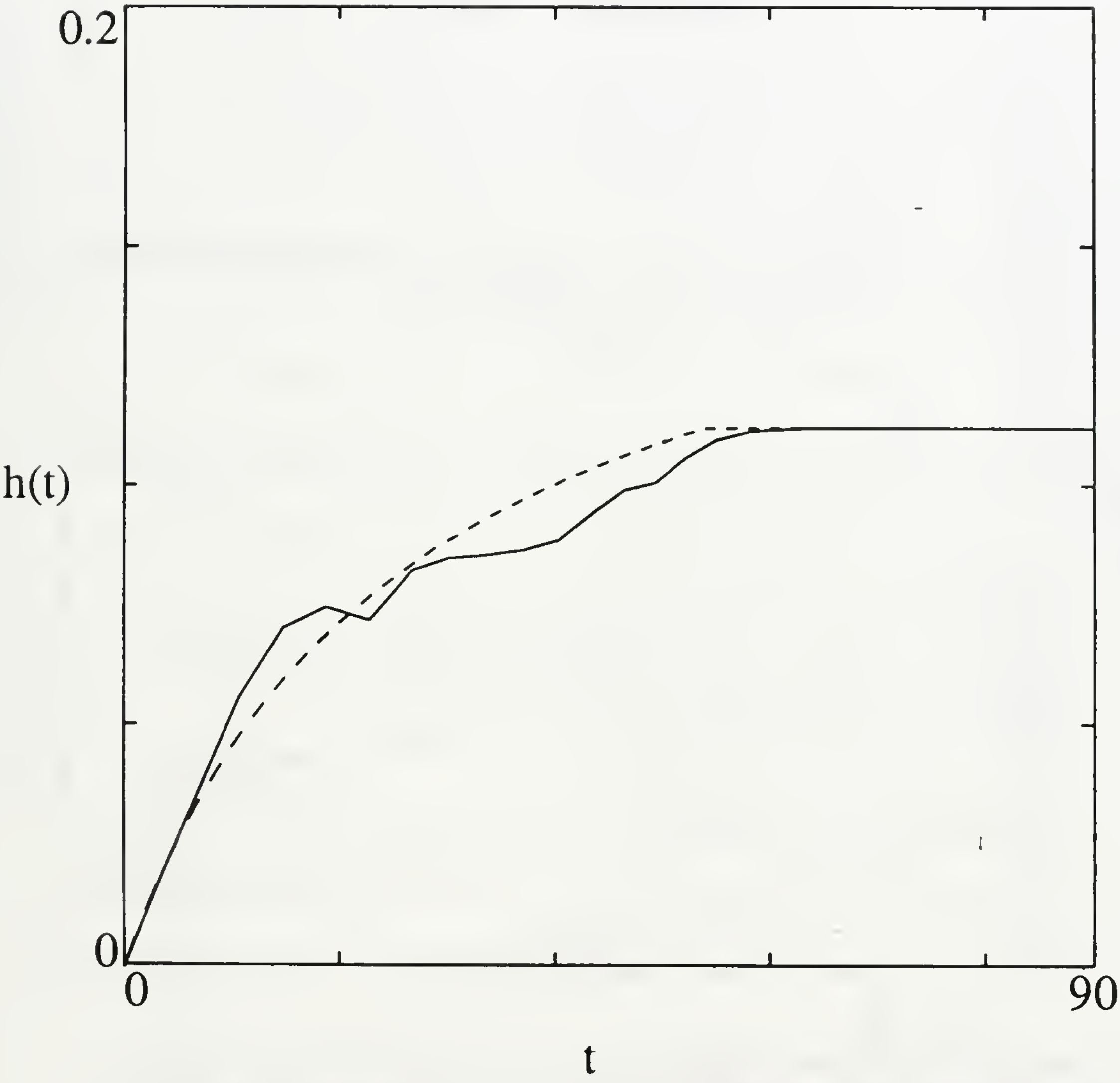

Figure 4.1a. The variation of finger height with time. The solid line and dashed line are the numerical and theoretical results.

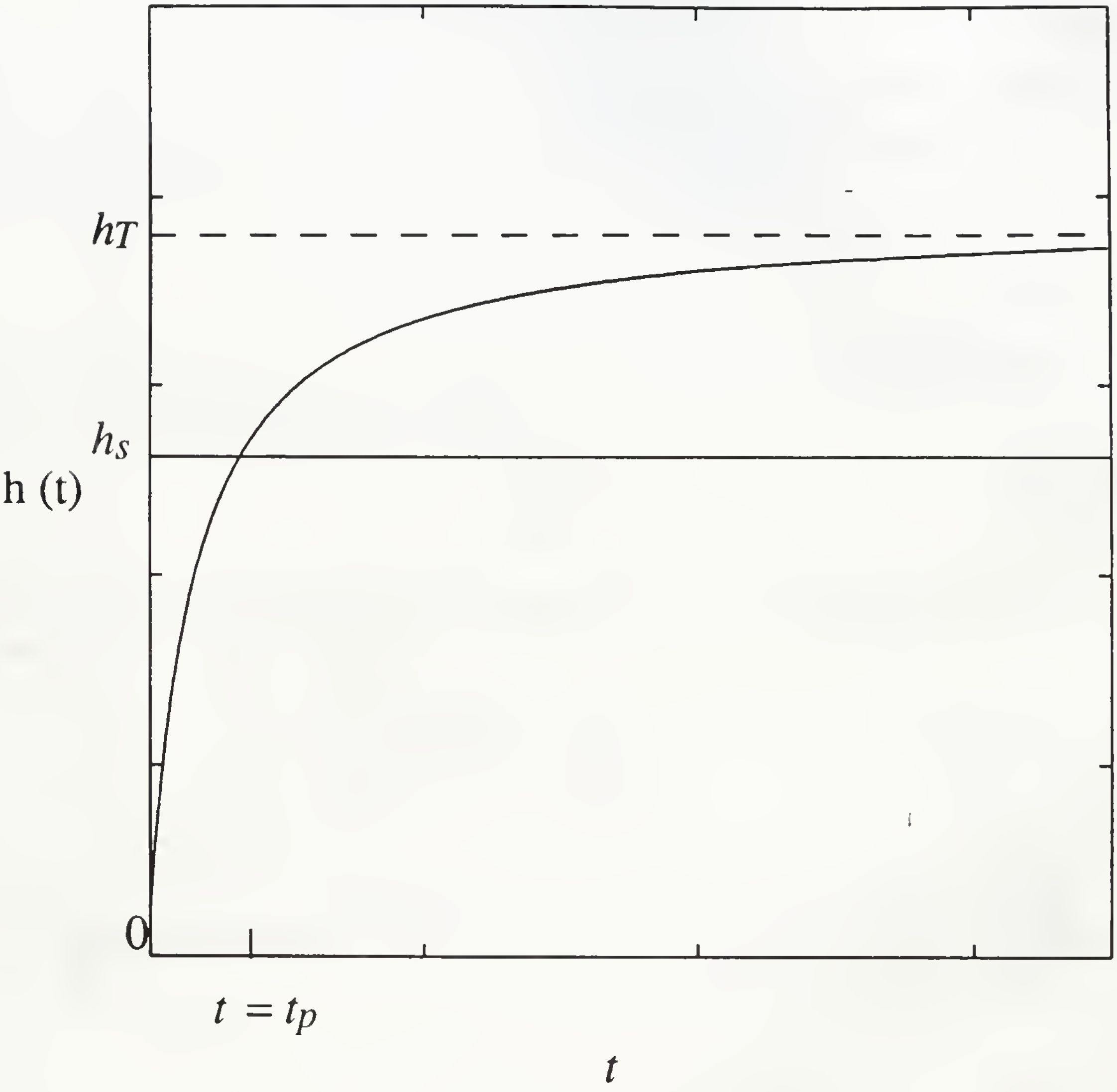

Figure 4.1b. The threshold finger height h_T. When the solvent channel height h_s satisfies $h_s < h_T$, pinch off occurs. When $h_s > h_T$ pinch off does not occur.

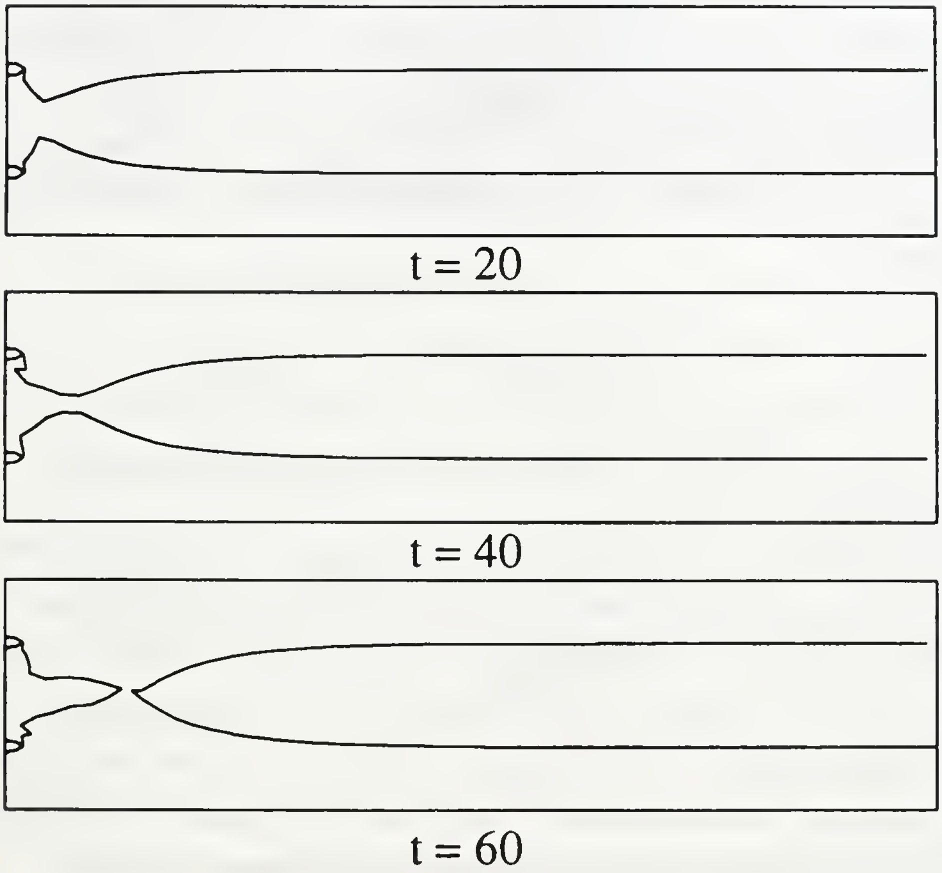

Figure 4.2a. The interface at times $t = 20, 40, 60$, before and near pinch off, are calculated by numerical simulation, for $V = 2$, $M = 5$ and $W = 0.82$. The mesh sizes are 70×40 hyperbolic and 150×70 elliptic.

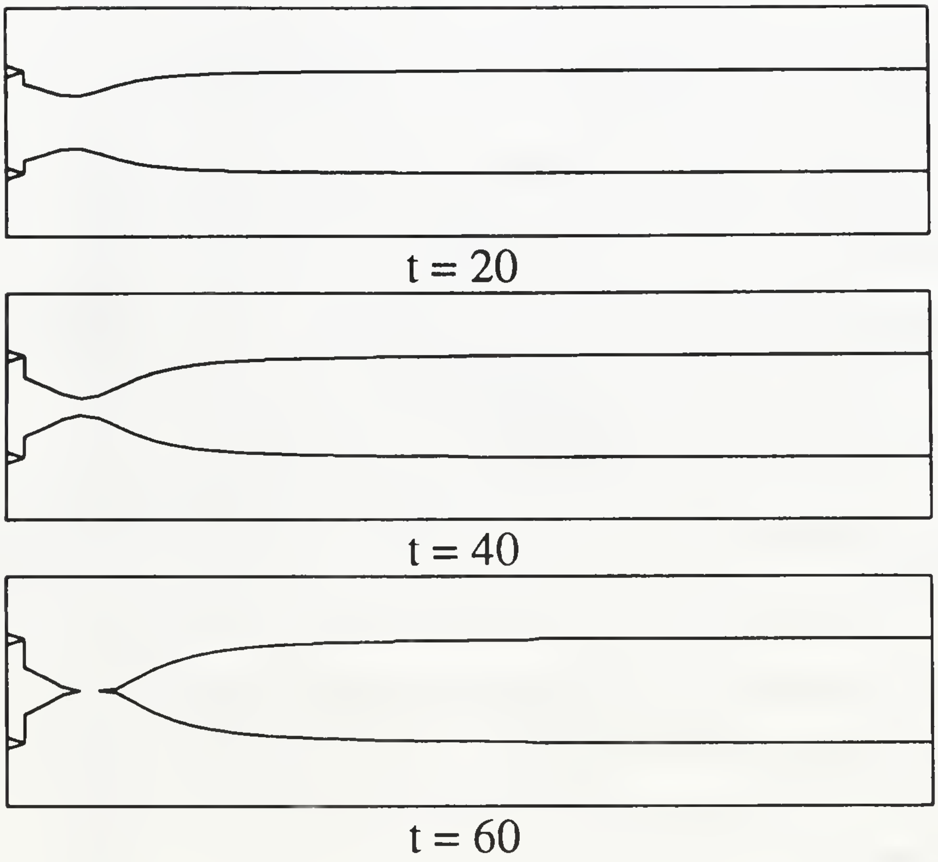

Figure 4.2b. The interface calculated by the theoretical model (4.1) at the same times and parameter values as were used in the simulation of Figure 4.2a.

The second time scale, t_s, is the characteristic time for a finger moving down stream to expand its width by an amount $2WH/\pi$,

$$t_s = \frac{2WH/\pi}{\zeta v'_s} \quad . \tag{4.9}$$

To give an order parameter approximately characterizing the flow pattern, we introduce the ratio β of the two time scales,

$$\beta = \frac{t_s}{t_p} = \frac{\left[\dfrac{4W\gamma_o}{3\pi} - \zeta(1-W)M\right]}{0.27\zeta M\,(1-W)} \quad . \tag{4.10}$$

For $\beta > 1$, the finger pinches off before it moves far enough downstream for new fingers to form. The consecutive pattern of pinch offs turns the flow stream into a series of slugs. For $\beta < 1$, the rate of finger growth on the interface is slowed down by its expansion. The fluctuations of the interface become increasingly significant and pinch off, even it occurs eventually, may not be predicted accurately by our model. When $\beta < 0$ the solvent channel width is above the threshold, pinch off, if it occurs, is a random event generated by the fluctuations. In this case the pinch off time is not well defined. We generalize (4.10) to classify the resulting chaotic flows by defining the amplitude δh of the fluctuation required for an oil finger to break the solvent channel,

$$\delta h = (1 - W) - \frac{h_T}{H} \quad .$$

Then (4.10) can be rewritten as

$$\beta = -\frac{\delta h}{0.27(1 - W)} = 3.7(x-1) \ , \quad x = \frac{h_T}{h_s} = \frac{4\gamma_o W}{3\pi\zeta M(1 - W)} \quad . \tag{4.11}$$

In the limit of laminar flow, we have $MV = 1$ and $0 = \gamma_0 = h_T = x$ and so $\beta = -3.7$. In summary we conclude that the laminar-slug flow transition occurs near $\beta = 0$ and in this region, the flow pattern is chaotic, with random pinch offs or multi-finger growth on the interface. For large positive β well developed slugs are formed. When β approaches -3.7, laminar flow results. Our simulation results indicate a qualitative agreement with this prediction for the nature of the phase plane. We summarize our simulation results in Table 4.1. In the laminar and chaotic flow limits, ζ is not well defined by our fitting procedure, and we have arbitrarily set $\zeta = 0.2$.

For $MV < 1$, i.e. $\gamma_o < 0$, there is excess solvent inflow. In the region of physical interest, V is positive, so $|\gamma_o|$ can not be too large. Moreover, the analysis of §3 shows that in this case, the fingers are transported slowly, grow on the down stream side, and the overall flow pattern converges to a steady state equilibrium of laminar flow. As result the pinch-off is unlikely in this case.

V	M	W	β	α_{th}	α_{num}	t_p	t'_p	Flow pattern
0.11	10	0.82	-0.34	-	-	-	-	Laminar flow
1	5	0.2	-1.4	-	-	-	-	Chaotic flow
2	5	0.4	0.1	-	-	-	-	Pinch off
1	10	0.92	4	0.25	0.20	20	20	Slug flow
0.33	15	0.92	2.1	0.64	0.55	31	28	Slug flow
1	5	0.92	3	0.31	0.4	39	37	Slug flow
1.43	15	0.82	2	0.24	0.15	35	33	Slug flow
2	5	0.82	2	0.23	0.15	54	58	Slug flow

Table 4.1. Values of slug size and flow regime order parameters α and β are tabulated for various simulations, to display the dependence on the velocity, mobility and width ratios V, M and W. α_{th} and α_{num} are the theoretical and numerical values for slug size in units of channel flow width. The theoretical and numerical values of the pinch off times, t_p and t'_p, respectively, are compared. For $W = 0.82$ we choose $\zeta = 0.21$ and for $W = 0.92$, $\zeta = 0.16$.

The numerical calculations of initial finger growth in the slug flow regime are not sensitive to the grid size, and converge under mesh refinement. At later times in the simulation, i.e. for the formation of multiple, repeated slugs, and their movement down stream, we find qualitatively similar pictures, differing in detail, as the mesh is refined. It appears that the use of an unregularized, unstable formulation of the physics is the cause and that the use of surface tension or other regularization would be required to obtain convergence. See Figures 4.3 and 4.4.

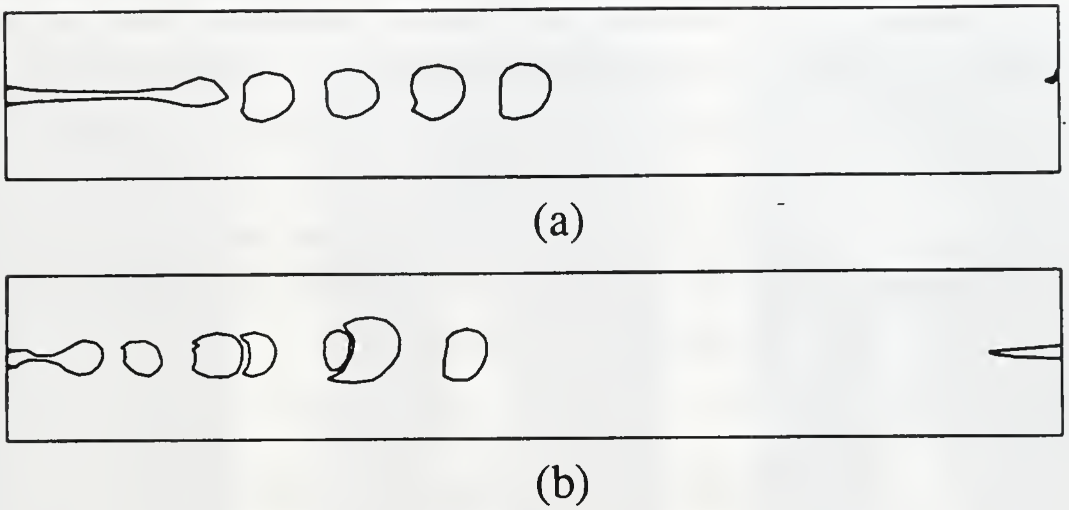

Figure 4.3. Consecutive pinch off turns a laminar flow into slug flow. Here $V = 1$, $M = 5$, $W = 0.92$ and $\beta = 2$. We compare distinct mesh sizes. (a) The mesh size is 42×14 for the hyperbolic equation, 84×30 and for the elliptic equation. (b) We repeat the calculation of (a) by using a refined mesh, which is 64×28 for the hyperbolic equation, 180×60 and for the elliptic equation.

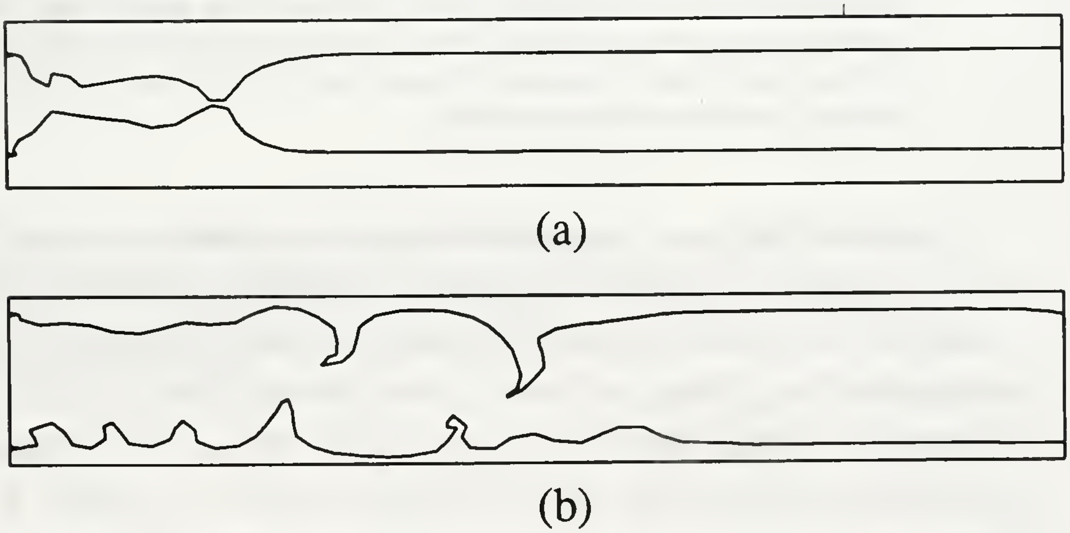

Figure 4.4. Comparison of distinct flow regimes. (a) The pinch off occurs in a random way. Here $V = 2$, $M = 5$, $W = 0.4$ and $\beta = 0.1$. (b) Chaotic flow without pinch off. Here $V = 1$, $M = 5$, $W = 0.2$ and $\beta = -1.4$. The mesh size for both cases is 30×10 for the hyperbolic equation, 60×30 and for the elliptic equation.

5. Variable Channel Width and Complex Barriers

As we show in Figure 5.1, even if the boundary conditions give steady laminar flow i.e. even if the velocity ratio is equal to its equilibrium value, the flow in the channel throat can be out of equilibrium. In this case an instability of the interface develops locally. Since the width ratio W and velocity ratio V change with variation of the channel width, β may change in a variable channel. In a region where β is positive and not too large, pinch off is favored, leading to a transition of laminar to slug flow. The point to our analysis is that the pinch off can occur upstream of, i.e. upon entering, the channel throat.

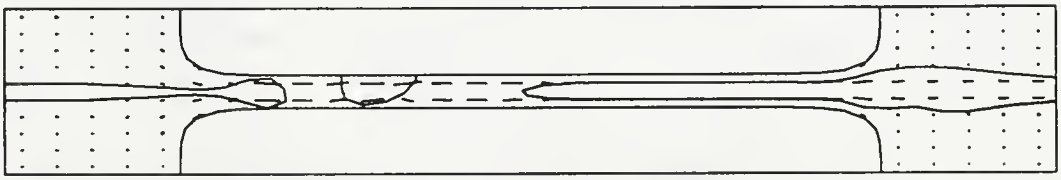

Figure 5.1. Both the inlet and outlet injection rates are set to their equilibrium values, i.e. $MV = 1$, where $M = 5$. However, two barriers in the middle produce a narrow flow channel and alter the velocity ratio, so that a change of flow pattern results. At the upstream side of barriers, V increases from 0.2 to 1.0 and value of β is 1.1. A transition from laminar to slug flow is observed. The mesh size is 60 × 20 for the hyperbolic equation, and 120 × 60 for the elliptic equation.

In the problem of two viscous fluids flowing among random arrays of barriers, the complex flow channels can give rise to competing flows which causes pinch-off as we discussed in previous sections. An idealized geometry which displays this effect is shown in Figure 5.2. First the solvent inflow is split by two front barriers, and then driven into a narrow channel. Because of the competing flow channel around the first barrier, the velocity ratio at the entrance to the second channel deviates from equilibrium values, i.e. $MV \neq 1$. Thus pinch off results and slugs are produced. In Figure 5.3, we show the results of numerical calculations of flow in a random array of barriers, perhaps more representative of reality. In this flow, pinch off appears to be associated with competing flow paths, as in Figure 5.2.

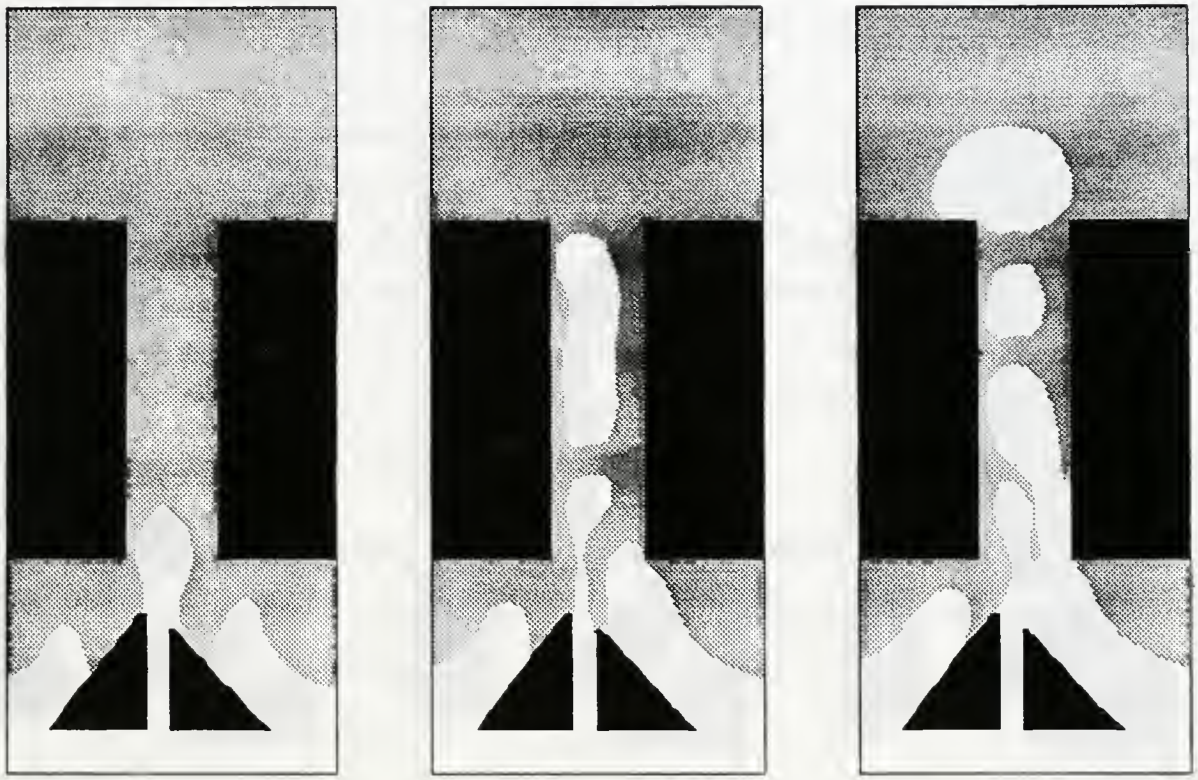

Figure 5.2. Numerical calculation of viscous flow of two fluids in a channel with complex geometry. The computation shows formation of competing flows and pinch off between barriers. We use gray scale to distinguish three different phases. The barrier, oil and solvent are shaded by black, gray and white.

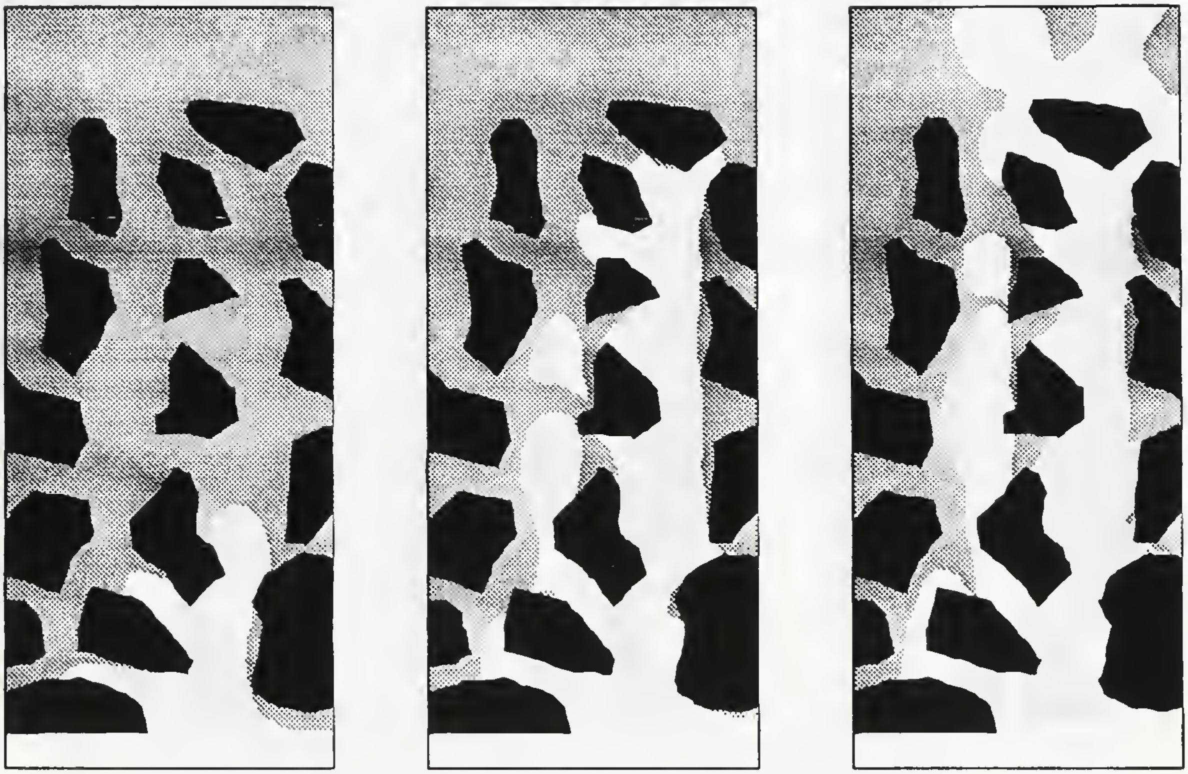

Figure 5.3. Miscible flood of an oil core containing an array of impermeable barriers approximating the microstructure of porous media. The boundary between the injected solvent phase and the displaced oil phase is shown at three different dimensionless times during the flood, from left to right $t =$ 1.1, 3.0 and 4.0. The mobility ratio $M = 10$. The competing oil and solvent flows cause pinch off. The barreiers, oil and solvent are shaded with black, gray and white.

6. Conclusions

We have studied the viscous flow of two fluids in a Hele-Shaw cell of complex geometry. We have shown that when the velocity ratio of the two fluids is not equal to its equilibrium value i.e. $MV \neq 1$, a new type of instability (i.e. fingers growing which have qualitative features not present in the classical Taylor-Saffman instability) develops. Using a simple theoretical model, we have studied the pinch off phenomena quantitatively. We are able to give the condition for the occurrence of pinch off and calculate pinch off time. An order parameter $\beta(V, M, W)$ is given to characterize the distinct flow pattern regimes and the transitions between them. We obtained agreement between analytic and simulation results. The transition of laminar to slug flow provides a possible mechanism for foam generation in enhanced oil recovery.

7. Appendix. The transverse velocity field of the nonuniform flow

To calculate the transverse velocity field of the nonuniform flow along the interface at $t = 0$, we start from the elliptic equations (A.1)

$$\nabla^2 P_i = 0 \ , \quad v_i = -\frac{1}{\mu} \nabla P_i \ , \quad i = 1,2 \tag{A.1}$$

with the boundary conditions

$$v_x(x=0,\, y) = \begin{cases} v_1, & y > 0 \\ v_2, & y < 0 \end{cases}$$

$$v_x(x=L,\, y) = \begin{cases} v'_1, & y > 0 \\ v'_2, & y < 0 \end{cases} \tag{A.2}$$

$$v_y(x,\, y=-WH) = v_y(x,\, y=H-WH) = 0 \quad .$$

The interface is located $y = 0$, at $t = 0$. For $k \neq 0$ the eigen-solutions of (A.1) have the form

$$P_1^k = A_k \cos[k(y-(1-W)H)] \cosh[k(L-x)] \ ,$$

$$P_2^k = B_k \cos[k(y+WH)] \cosh[k(L-x)] \quad . \tag{A.3}$$

For $k = 0$

$$P_i = C_i x, \qquad i = 1,2$$

where A_k, B_k and C_i are constants. The condition of continuity of pressure and normal velocity at the interface gives

$$P_1^k(y=0) = P_2^k(y=0) \quad ,$$

$$\frac{1}{\mu_1}\frac{\partial}{\partial y}P_1(y=0) = \frac{1}{\mu_2}\frac{\partial}{\partial y}P_2(y=0) \quad . \tag{A.4}$$

From (A.3) and (A.4), the eigen-frequences of $k = k_n$ can be determined from the equation

$$\sin k_n H = \frac{\mu_2 - \mu_1}{\mu_2 + \mu_1}\sin[k_n(1-2W)H] \quad . \tag{A.5}$$

The solution of (A.1) under the boundary condition (A.2) can be written as

$$P_1 = -\mu_1 v_1 x + \sum_n \mu_1 \frac{2(\mu_1\delta v_1 - \mu_2\delta v_2)}{\mu_1\sin^2(k_nWH) + \mu_2\sin^2[k_n(1-W)H]}\frac{1}{k_n^2}\sin^2(k_nWH)$$

$$\times \sin[k_n(1-W)H]\cos[k_ny - k_n(1-W)H]\frac{\cosh\,[k_n(L-x)]}{\sinh\,k_nL} \tag{A.6}$$

and

$$P_2 = -\mu_2 v_2 x - \sum_n \mu_2 \frac{2(\mu_1\delta v_1 - \mu_2\delta v_2)}{\mu_1\sin^2(k_nWH) + \mu_2\sin^2[k_n(1-W)H]}\frac{1}{k_n^2}\sin^2[k_n(1-W)H]$$

$$\times \sin(k_nWH)\cos[k_n(y+WH)]\frac{\cosh\,[k_n(L-x)]}{\sinh\,k_nL} \tag{A.7}$$

where

$$\delta v_i = v_i - v'_i \quad .$$

We obtain the expression for transverse velocity v_y

$$v_y(x,\, y=0) = -\sum_n \frac{2(\mu_1\delta v_1 - \mu_2\delta v_2)}{\mu_1\sin^2(k_nWH) + \mu_2\sin^2[k_n(1-W)H]}\frac{1}{k_nH}$$

$$\times \sin^2(k_nWH)\sin^2(k_n(1-W)H)\frac{\cosh\,[k_n(L-x)]}{\sinh k_nL} \quad . \tag{A.8}$$

When $L \to \infty$, we have

$$v_y(x,\ y=0) = -\sum_n \frac{2(\mu_1 \delta v_1 - \mu_2 \delta v_2)}{\mu_1 \sin^2(k_n WH) + \mu_2 \sin^2[k_n(1-W)H]} \frac{1}{k_n H}$$

$$\times \sin^2(k_n WH) \sin^2(k_n(1-W)H) \exp(-k_n x) \qquad \text{(A.9)}$$

We discuss the solutions of (A.9) in some special cases.

i) When $W = \frac{1}{2}$, from (A.5) we have

$$\sin k_n H = 0\,, \qquad k_n = \frac{n\pi}{H}$$

$$\sin(k_n WH) = \sin\frac{n\pi}{2} = \begin{cases} 0, & n = 2k \\ (-1)^k, & n = 2k+1 \end{cases} \qquad \text{(A.10)}$$

$$\sin(k_n(1-W)H) = \sin\frac{n\pi}{2} = \begin{cases} 0, & n = 2k \\ (-1)^k, & n = 2k+1 \end{cases}\ ,$$

and thus

$$v_y = -\frac{2(\mu_1 \delta v_1 - \mu_2 \delta v_2)}{\mu_1 + \mu_2} \sum_n \frac{1}{(2n+1)\pi} \exp[-(2n+1)\pi x/H]$$

$$= -\frac{(\mu_1 \delta v_1 - \mu_2 \delta v_2)}{\pi(\mu_1 + \mu_2)} \ln \frac{1 + \exp(-\pi x/H)}{1 - \exp(-\pi x/H)} \qquad \text{(A.11)}$$

ii) For $\mu_2 \gg \mu_1$, from (A.5) we have

$$\sin k_n H = -\sin k_n (1 - 2W) H \qquad \text{(A.12)}$$

so that

$$k_n = \frac{(2n+1)\pi}{2WH}\ .$$

We obtain

$$v_y = -\sum_n \frac{2(\mu_1 \delta v_1 - \mu_2 \delta v_2)}{\mu_1 + \mu_2 \cos^2[(n+\frac{1}{2})\frac{\pi}{W}]} \cos^2[(n+\frac{1}{2})\frac{\pi}{W}] \frac{2W}{(2n+1)\pi} \exp[-(2n+1)\pi/2WH]$$

$$\approx \delta v_2 \frac{2W}{\pi} \ln \frac{1+\exp(-\pi x/2WH)}{1-\exp(-\pi x/2WH)} \quad . \tag{A.13}$$

References

1. H. B. Stewart and B. Wendroff , "Two-Phase Flow: Models and Methods," *J. Comp. Phys., vol. 56* , pp. 363-409 , 1984 .
2. *Advances in Multiphase Flow and Related Problems*, Ed. G. Papanicolaou, SIAM, Philadelphia, 1986.
3. C. Gardner, J. Glimm, O. McBryan, R. Menikoff, D. H. Sharp, and Q. Zhang, "The Dynamics of Bubble Growth for Rayleigh-Taylor Unstable Interfaces," *Phys. of Fluids*, vol. 31, pp. 447-465, 1988.
4. J. Glimm, E. Isaacson, D. Marchesin, and O. McBryan, "Front Tracking for Hyperbolic Systems," *Advances in Appl. Math.*, vol. 2, pp. 91-119, 1981.
5. J. Glimm, X. L. Li, R. Menikoff, D. H. Sharp, and Q. Zhang, *Statistical Theories of Rayleigh-Taylor Instability for Compressible Fluids*, To appear.
6. D. G. Huh, T. D. Cochrane, and F. S. Kovarik, "The effect of microscopic heterogeneity on CO_2 / foam mobility. Part I -- a mechanistic study," SPE/DOE 17359, 1988.
7. K. I. Read, "Experimental Investigation of Turbulent Mixing by Rayleigh-Taylor Instability," *Physica 12D*, pp. 45-48, 1984.
8. P. G. Saffman and G. I. Taylor, "The penetration of a fluid into a porous medium or Hele-Shaw cell containing a more viscous liquid," *Proc. Royal Soc. London*, vol. A245 , pp. 312-329, 1958.
9. D. H. Sharp and J. A. Wheeler, "Late Stage of Rayleigh-Taylor Instability," Institute for Defense Analyses, 1961.
10. D. H. Sharp, "Overview of Rayleigh-Taylor Instability," *Physica 12D*, pp. 3-17, 1984.
11. B. I. Shraiman and D. Bensimon, "Singularities in nonlocal interface dynamics," *Phys. Rev.* , vol. A 30, p. 2840, 1984.

12. A. P. Szilas, *Production and transport of oil and gas*, pp. 100-106, Elsevier Scientific Publishing Company, 1975.

13. G. B. Wallis, *One-dimensional Two-phase Flow*, McGraw-Hill Book Company, 1969.

14. Juan A. Zufiria, ''Bubble Competition in Rayleigh-Taylor Instability,'' *Phys. of Fluids*, vol. 31, pp. 440-446, 1988.

NYU DOE/ER 25053-2
Glimm, James
The laminar to slug flow transition in Hele-Shaw flow.
c.2

This book may be kept
FOURTEEN DAYS
A fine will be charged for each day the book is kept overtime.

GAYLORD 142
PRINTED IN U.S.A.